Birdsell et al. 2000

ELSEVIER

Journal of Contaminant Hydrology 46 (2000) 99–129

JOURNAL OF Contaminant Hydrology

www.elsevier.com/locate/jconhyd

Groundwater flow and radionuclide transport calculations for a performance assessment of a low-level waste site ☆

Kay H. Birdsell [a,*], Andrew V. Wolfsberg [a], Diana Hollis [a], Terry A. Cherry [a], Kathleen M. Bower [b]

[a] *Los Alamos National Laboratory, Los Alamos, NM 87545, USA*
[b] *Eastern Illinois University, Charleston, IL 61920, USA*

Received 23 February 1999; received in revised form 12 June 2000; accepted 27 June 2000

Abstract

Predictions of subsurface radionuclide transport are used to support the groundwater pathway analysis for the performance assessment of the low-level, solid radioactive waste site at Los Alamos National Laboratory. Detailed process-based models rather than higher-level performance-assessment models are used to perform the transport calculations. The deterministic analyses predict the fate of the waste from its source, through the vadose zone, into the saturated zone and, finally, the potential dose to humans at the accessible environment. The calculations are run with the finite-element code FEHM, which simulates fluid flow, heat transport, and reactive, contaminant transport through porous and fractured media.

The modeling approach for this study couples realistic source-term models with an unsaturated-zone flow and transport model, which is then linked to the saturated-zone flow and transport model. The three-dimensional unsaturated-zone flow and transport model describes the complex hydrology associated with the mesa-top and volcanic geology of the site. The continued migration of nuclides into the main aquifer is calculated using a three-dimensional, steady-flow, saturated-zone model that maintains the spatial and temporal distribution of nuclide flux from the vadose

☆ Note: Most of the Los Alamos National Laboratory Publications are available on the web site http://lib-www.lanl.gov/pubs/la-pubs.htm.

* Corresponding author. Fax: +1-505-665-8737.
E-mail addresses: khb@lanl.gov (K.H. Birdsell), awolf@lanl.gov (A.V. Wolfsberg), dhollis@lanl.gov (D. Hollis), tam@lanl.gov (T.A. Cherry), cfkmb1@eiu.edu (K.M. Bower).

0169-7722/00/$ - see front matter
PII: S0169-7722(00)00129-7

zone. Preliminary results for the aquifer-related dose assessments show that doses are well below relevant performance objectives for low-level waste sites.

A general screening technique that compares the nuclide's half-life to its unsaturated-zone travel time is described. This technique helps to decrease the number of transport calculations required at a site. In this case, over half the nuclides were eliminated from further consideration through this screening.

Keywords: Performance assessment; Hydrology; Radioactive waste; Unsaturated zone

1. Introduction

Environmental and human-health concerns associated with radionuclides in groundwater are a legacy of nuclear energy and nuclear weapons development over the last 50 years. Risk analyses and performance assessments for radioactive waste disposal sites rely heavily on transport calculations that predict the migration of radionuclides through the subsurface over thousands of years. This paper presents an integrated case study that predicts the groundwater pathway dose for the performance assessment (PA) of the active, low-level, solid radioactive waste site located at Los Alamos National Laboratory (LANL) in northern New Mexico, as shown in Fig. 1.

Specifically, performance assessment is required to site and authorize permanent disposal facilities for radioactive waste. The purpose of the PA is to demonstrate that performance measures related to protection of human health and the environment are not likely to be exceeded for a specified period of time. Performance objectives and periods of compliance vary according to the characteristics of the radioactive waste being disposed, but groundwater protection for U.S. sites is always explicitly required for at least 1000 years.

The general PA approach is shown with the triangular diagram in Fig. 2 (U.S. Department of Energy, 1998). At the bottom of the triangle, the process starts with the gathering of site characterization data. At the next tier, these data are synthesized into a conceptual model that summarizes the current understanding of the processes that control radionuclide migration at the site. Numerical or analytical models are then used to study these processes in order to gain insight into, for example, the relative magnitude of various processes. The models at this second tier can be quite detailed process-level models. At the third tier of the triangle, PA models are generally abstracted from the detailed models by simplifying processes or pathways. However, a high level of complexity may be retained at the PA level if deemed necessary (U.S. Department of Energy, 1998).

Finally, the top tier of the triangle represents the total system performance assessment (TSPA) where the individual PA models are coupled to simulate the total system. The TSPA may use a deterministic approach, but probabilistic analyses are usually employed. An important feature of the PA process is its iterative nature. Information needs can be identified and additional information gathered at any tier throughout the process, thus reducing uncertainty in the performance predictions. Although the diagram in Fig. 2

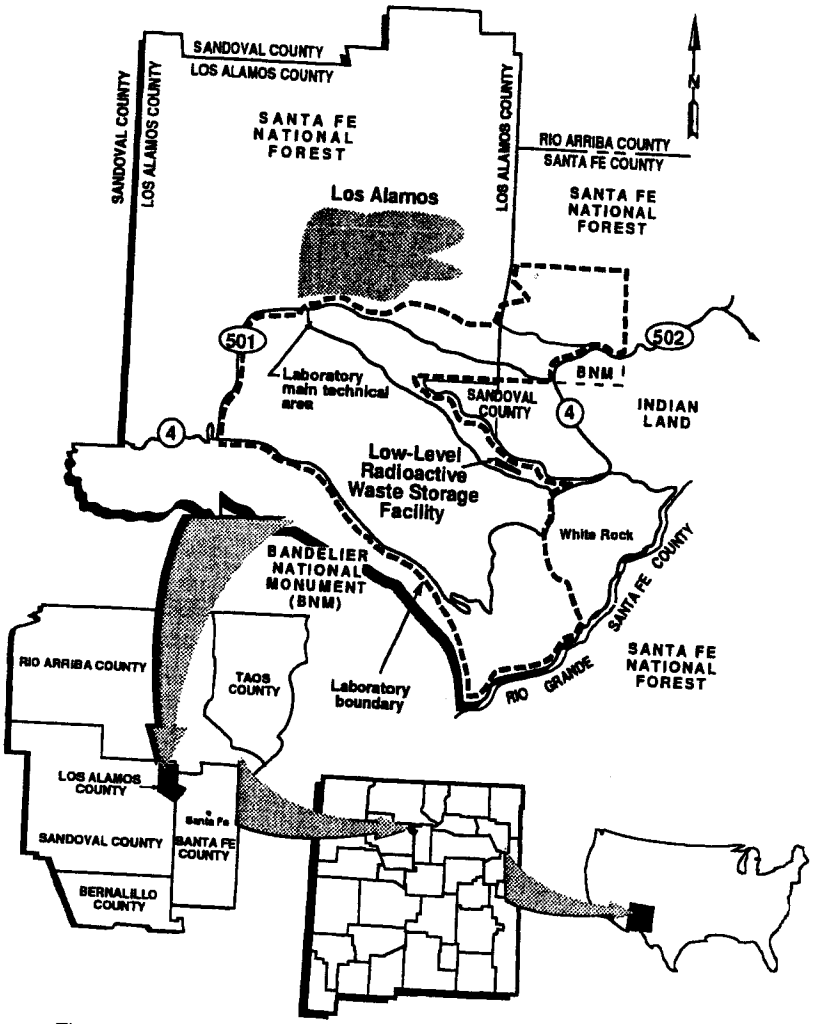

Fig. 1. Location of the low-level waste site at Los Alamos National Laboratory.

is based on the DOE's approach to performance assessment, the international community (Thompson, 1999) and the U.S. Nuclear Regulatory Commission (Eisenberg et al., 1999) use similar approaches.

Whereas PA calculations generally do not explicitly incorporate detailed processes and site-characterization data (e.g., Wilson et al., 1994), this case study does. We demonstrate the incorporation of site data into a conceptual model, and the use of process-level models to evaluate the effects of phenomena such as transient flow and fracture transport on aqueous transport through the unsaturated zone. The final perfor-

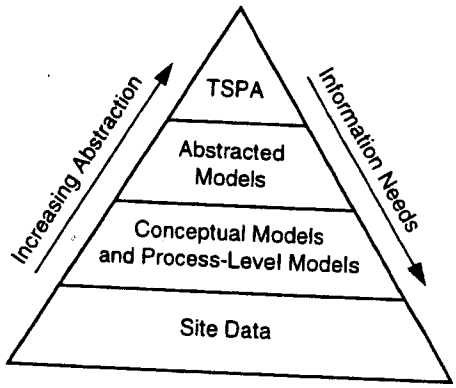

Fig. 2. Performance assessment methodology (based on U.S. Department of Energy, 1998).

mance calculations use models that are abstracted from the more complex phenomenological models, although they remain at the process level. The models are used to calculate the source release of the waste, the continued migration of the waste through the unsaturated and saturated zones, and the potential aquifer-related doses to human receptors. An advantage of using process models throughout the analysis is that a strong link is maintained between the numerical model and the conceptual model.

The three-dimensional unsaturated-zone flow and transport model captures the complex hydrogeology and topography of the site and yields radionuclide flux estimates to the regional aquifer. Within the unsaturated-zone model, the source release of radionuclides is computed for 38 waste disposal pits and four shaft fields, each contributing to the total inventory. The continued migration of radionuclides through the aquifer is calculated using a three-dimensional model designed to maintain the temporally and spatially varying distribution of radionuclide flux from the unsaturated zone. Finally, groundwater concentrations are converted to aquifer-related doses. This dose information, along with information predicted for other exposure pathways, is included in the site TSPA.

All calculations were run with the finite-element code FEHM, which simulates single- and multi-phase fluid flow and reactive contaminant transport through porous and fractured media (Zyvoloski et al., 1997). General screening and scaling techniques, which help to make site assessment with process-level models tractable by reducing the number of contaminants requiring full analyses, are also presented.

The modeling approach described passed comprehensive technical and regulatory reviews, as required by the DOE, and the PA was approved as the technical basis for LANL's authorization to continue on-site disposal. Because of its successful application to the PA, the same groundwater flow and transport modeling approach is being used to support groundwater-pathway risk assessments and remedy evaluation for several other formerly used disposal sites at the LANL. Using already tested and proven models is expected to significantly streamline the corrective-action process for these formerly used radioactive waste disposal sites.

2. Site description

2.1. Stratigraphy and topography

The strata that underlie the LANL waste site are composed of a series of nonwelded to moderately welded rhyolitic ash-flow and ash-fall tuffs underlain by a thin pumice bed, a thick basalt, and a conglomerate formation (Krier et al., 1997) as shown in Fig. 3. The tuff layers were deposited during violent eruptions of volcanic ash from the Valles Caldera some 1.2 to 1.6 million years ago (Smith and Bailey, 1966; Gardner et al., 1986). Since then, the tuff has eroded to leave a system of alternating finger-shaped mesas and canyons. LANL's low-level waste disposal facility is located atop one such mesa with the waste buried in disposal pits and shafts to a depth of approximately 20 m. The surrounding canyons lie 30 m below the steep-sided mesa, and the water table is located approximately 250 to 300 m below the disposal pits.

The upper six stratigraphic units make up the Bandelier Tuff. These units dip gently and thin toward the eastern end of the site. The top tuff layer, Unit 2, and the upper few

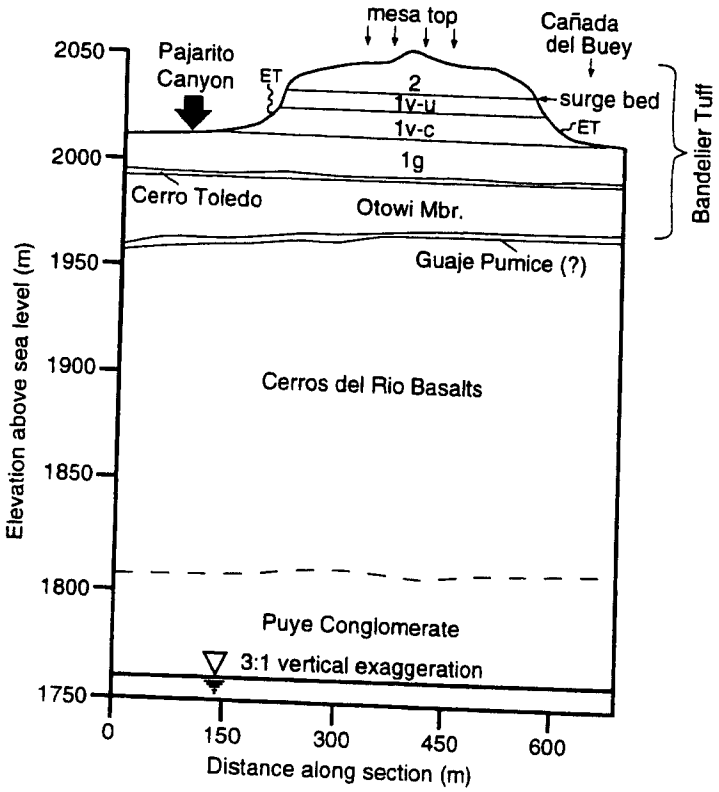

Fig. 3. Two-dimensional site stratigraphy (Krier et al., 1997) with boundary conditions for the unsaturated-zone simulations. The arrows show infiltration and evapotranspiration regions with their size reflecting relative magnitude.

meters of the second layer, Unit 1v-u, are extensively fractured and are separated by a thin surge bed (Krier et al., 1997). The surge bed is made up of fine, sand-sized material and is genetically related to the overlying deposits of poorly sorted, relatively massive ashflow tuff (Fisher, 1979). The deeper tuff units have few observed fractures in outcrop (Krier et al., 1997).

The Cerros del Rio Basalts, which comprise over 50% of the unsaturated zone, display wide variability (Turin, 1995). The basalts range from extremely dense with no apparent porosity, to highly fractured, to so vesicular as to appear foamy. The Puye Conglomerate lies at the base of the unsaturated zone and extends into the saturated zone. The conglomerate consists of cobbles and boulders of volcanic debris in a matrix of silts, clays, and sands (Purtymun, 1995). Clay, silt and pumice lenses, and interbedded basalts are also common.

2.2. Contaminant source

The waste disposal facility occupies about 300,000 m^2 atop a finger-shaped mesa with waste buried in pits and shafts to a depth of approximately 20 m. In the pits, the waste is layered and compacted to improve stability, and void spaces are backfilled with crushed tuff to minimize subsidence. A typical pit contains at least 60% consolidated crushed tuff (Hollis et al., 1997). Between 1957 and 1995, solid radioactive waste was buried in 34 disposal pits and in almost 200 shafts located in five shaft fields. The waste form buried at the site contains over 60 radionuclides with the majority of the waste being ^{235}U, ^{238}U, and ^{232}Th. Currently, only low-level radioactive waste is accepted, but prior to 1971, transuranic and mixed waste were also accepted (Shuman, 1997a). An expansion area with four large pits and another shaft field is planned for operation through 2044 and is included in this study.

The oldest wastes are buried at the eastern-most portion of the site, and disposal operations have proceeded toward the west (see Fig. 4). The waste is categorized in terms of four disposal-unit classifications that are determined by the age of the wastes, because different regulations govern wastes disposed of during different time periods and because inventory records have improved with time. Whereas the performance assessment (PA) evaluates the releases for the 1988–1995 and projected 1996–2044 wastes, the composite analysis (CA) evaluates releases from all wastes, past and future. Detailed inventory information for the 1971–1988 waste and the 1988–1995 waste are obtained from disposal records. However, detailed inventory data are not available prior to 1971 and are uncertain for future activities. Therefore, the inventory in the 1957–1970 waste is extrapolated backwards based on disposal operations from 1971 to 1977, and the inventory for the 1996–2044 waste is projected based on current operations and expected future operations (Shuman, 1997a; Vold and Shuman, 1996).

2.3. Hydrologic data

The van Genuchten model (van Genuchten, 1980) is used to represent the moisture retention characteristic curves for all units in the unsaturated-zone model. Table 1 summarizes the hydrologic parameters used for all of the units in the unsaturated-zone

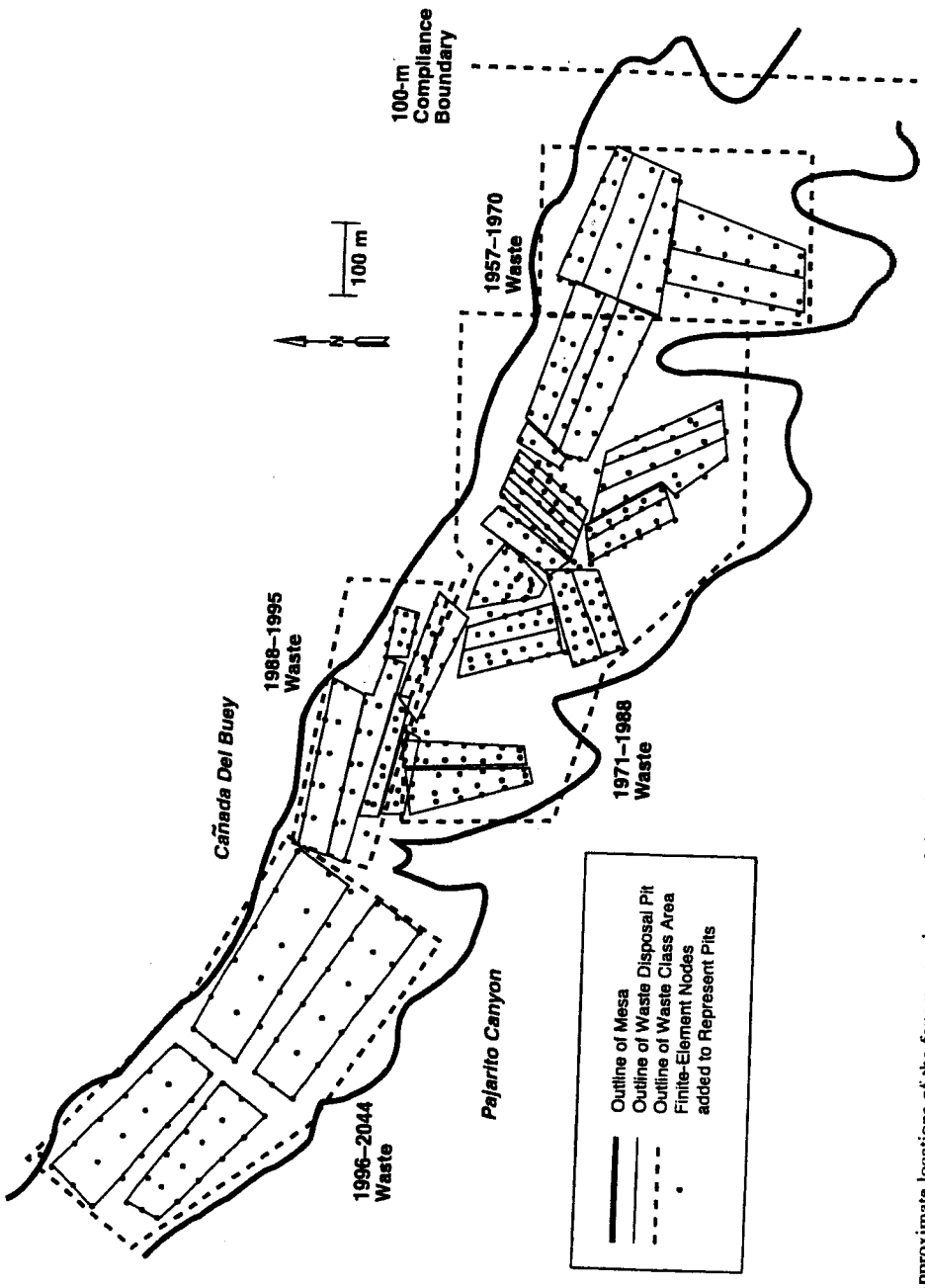

Fig. 4. Approximate locations of the four waste classes and the 100-m compliance boundary. Also shown are the pit boundaries, internal pit nodes, and the outline of the mesa edge for the three-dimensional unsaturated-zone grid.

Table 1
Hydrologic properties

Unit	K_{sat} (cm/s)	Porosity	van Genuchten θ_r, α (cm^{-1}), n
Pit (crushed Unit 2 tuff)[a]	2.89×10^{-4}	0.479	0.00767, 0.00663, 2.00389
Unit 2[b]	4.27×10^{-4}	0.481	0.013, 0.0060, 1.890
Unit 1v-u[b]	1.48×10^{-4}	0.517	0.002, 0.0030, 1.932
Unit 1v-c[b]	1.67×10^{-4}	0.509	0.009 0.0044, 1.647
Unit 1g[b]	1.88×10^{-4}	0.480	0.006, 0.0053, 1.745
Cerro Toledo[b]	8.65×10^{-4}	0.473	0.008, 0.0152, 1.506
Otowi Member[b]	2.49×10^{-4}	0.435	0.0188, 0.0059, 1.713
Guaje Pumice[a]	1.5×10^{-4}	0.667	0.0, 0.00081, 4.0264
Puye Formation[c,d]	4.6×10^{-3}	0.25	0.045, 1.45, 2.68
Cerros del Rio basalts (equivalent continuum)			
matrix properties[e]	9.7×10^{-5}	1×10^{-4}	6.6×10^{-6}, 0.0384, 1.474
fracture properties	9.7×10^{2}	1×10^{-4}	3.0×10^{-6}, 0.0384, 1.474

Bishop (1991).
[a] Springer (personal communication).
[b] Mean values from Krier et al. (1997).
[c] Purtymun (1984).
[d] Carsel and Parrish (1988).
[e] Bishop (1991).

flow and transport model. Hysteresis is not included. The parameters for the van Genuchten model (saturated permeability, porosity, inverse air entry pressure, etc.) are fairly well characterized for the six Bandelier Tuff units and for the crushed-tuff backfill but not for the deeper units. The properties for the tuff units (Krier et al., 1997), the crushed tuff, and the Guaje Pumice were measured on core samples of matrix material. Estimated values for the saturated conductivity and porosity of the Puye Conglomerate (Purtymun, 1984) are used, and we assume that the van Genuchten fitting parameters are similar to those of a coarse sand.

No hydrologic property data were available for the basalts at the time this study was performed. The basalt is modeled as a composite-continuum medium made up of both fractures and matrix material (Peters and Klavetter, 1988). To insure conservatism, we set the continuum porosity of the basalt to that of the fractures, thus forcing very low residence times of solutes in this unit for which we had no characterization data.

The upper-two tuff units are fractured and extremely dry as demonstrated by the site data in Fig. 5. Site data indicate that evaporation is an important process within the mesa top. These data include low mesa-top moisture contents (Krier et al., 1997) and high matrix potential measured along the surge bed (Rogers et al., 1996). Also, chloride and $\delta^{18}O$ profile analyses indicate strong evaporative effects yielding low, net water flux rates (Newman, 1996). For example, high porewater chloride concentrations observed in the mesa lead to flux estimates ranging from 0.03 to 1.5 mm/year while chloride concentrations below the canyon level yield fluxes near 5 mm/year (Newman, 1996). Previous numerical simulations indicate that evaporative effects can reasonably account for the low moisture contents observed in undisturbed regions of the mesa at the site and can justify a low net percolation rate (Birdsell et al., 1999).

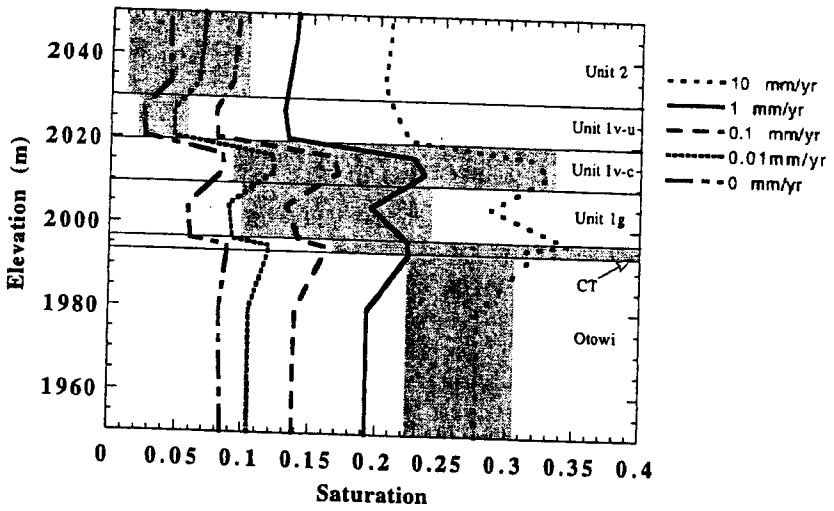

Fig. 5. Comparison of site data (gray boxes) to calculated steady-state saturation profiles for several infiltration rates. Calculated profiles are located at the center of the two-dimensional cross section in Fig. 3.

2.4. Transport properties

Distribution coefficients (K_d values) for americium, neptunium, plutonium, technetium and uranium were measured under saturated conditions with local rock samples using synthetic solutions representing local porewaters from the unsaturated zone and the aquifer (Longmire et al., 1996). However, K_d values for the remaining nuclides are based on experiments performed for the Yucca Mountain project (as summarized by Krier et al., 1997) and are not differentiated by tuff integrity or location. The K_d values for all nuclides considered in this study are shown in Table 2. Solubility limits for americium, plutonium and neptunium are based on experiments with Yucca Mountain tuffs and synthetic water samples with chemistry similar to either natural groundwaters at Yucca Mountain or at LANL (Longmire et al., 1996). Other solubility limits are derived from the literature (Krier et al., 1997). Solute speciation simulations based on porewater composition and pH and on tuff mineralogy were performed to ensure the applicability of the distribution coefficients and solubility limits used in the study (Longmire et al., 1996).

Site-specific measurements for diffusion coefficients and dispersivity are not available. We therefore estimate values of these parameters. Recent studies by Conca and Wright (1992) show that the diffusion coefficient decreases as moisture content decreases. For the unsaturated zone, the diffusion coefficient is modeled in this fashion and decreases parabolically from 10^{-9} m^2/s at saturation to 10^{-15} m^2/s at a moisture content of 0.001. For the saturated zone, the diffusion coefficient is assumed to be 10^{-9} m^2/s, consistent with the unsaturated-zone model at full saturation.

In the unsaturated zone, the dispersivity used is 1 m in the vertical direction and 0.1 m in the horizontal plane. Larger dispersivity values of 20 m in the direction of flow and 2 m transverse to the flow are used for the saturated zone because field studies have

Table 2
Median distribution coefficients (K_d (ml/g) for nuclides on intact and crushed tuff samples and on aquifer samples

	Intact tuff	Crushed tuff	Aquifer
Nonsorbing nuclides			
$^{99}Tc^a$	0	0	0
^{14}C, $^{129}I^b$	0	0	0
Weakly sorbing nuclides			
$^{237}Np^a$	2.25	7.5	0.151
^{233}U, ^{234}U, ^{235}U, ^{236}U, $^{238}U^a$	2.43	2.61	4.85
$^{93}Mo^b$	4	4	4
^{238}Pu, ^{239}Pu, ^{240}Pu, ^{241}Pu, $^{242}Pu^a$	4.13	711	13.95
Strongly sorbing nuclides			
$^{40}K^b$	15	15	15
$^{210}Pb^b$	25	25	25
$^{32}Si^b$	35	35	35
^{244}Cm, ^{152}Eu, ^{154}Eu, ^{148}Gd, ^{231}Pa, ^{147}Sm, $^{151}Sm^b$	50	50	50
$^{113m}Cd^b$	80	80	80
$^{108m}Ag^b$	90	90	90
^{93m}Nb, $^{94}Nb^b$	100	100	100
$^{90}Sr^b$	116	116	116
^{227}Ac, ^{249}Cf, $^{252}Cf^b$	130	130	130
^{226}Ra, $^{228}Ra^b$	200	200	200
$^{137}Cs^b$	428	428	428
^{182}Hf, ^{229}Th, ^{230}Th, ^{232}Th, $^{44}Ti^b$	500	500	500
$^{133}Ba^b$	946	946	946
^{241}Am, $^{243}Am^a$	2359	2050	141

[a] Site-specific values (Longmire et al., 1996).
[b] From Yucca Mountain experiments (Krier et al., 1997).

shown that dispersivity in the saturated zone increases with scale (Neuman, 1990; Gelhar et al., 1992). These are estimated using an empirical fit to field data developed by Neuman (1990) based on a length scale of approximately 100 m, the distance from the site boundary to the compliance point.

3. Conceptual model

The site conceptual model includes spatially variable infiltration, mobilization and release of radionuclides from the pits and shafts, migration of radionuclides through the unsaturated, fractured tuff, and finally transport in the saturated zone.

3.1. Infiltration and unsaturated-zone flow

The average precipitation rate for the area is 35.6 cm/year (Bowen, 1990). Most of this precipitation is lost to runoff and evapotranspiration, resulting in a heterogeneous infiltration pattern that is controlled by the mesa/canyon setting of the site. Infiltration is thought to be seasonal with most occurring during spring snowmelt and, to a lesser

extent, during the summer thunderstorm season (Rogers et al., 1997). Fig. 3 shows the different regions in which infiltration occurs. Based on measured rock saturations and chloride data, a very low net percolation rate (1 to 10 mm/year) is thought to exist within the mesa. Pajarito Canyon is wetter with an estimated percolation rate of 10 to 100 mm/year, while Cañada del Buey is dry with a percolation rate similar to the mesa top. The steep mesa sides represent an evaporative region (water sink) rather than a source region. The coupling of the fractured units separated by the high-permeability surge bed with the mesa's topographic relief is thought to enhance air circulation and consequently evaporative drying within the mesa interior. However, pit excavation through the upper two units destroys both the fracture network and the continuity of the surge bed, which likely disrupts the mesa's natural capacity for subsurface evaporation.

Matrix flow is expected to dominate in the unsaturated tuff units at the site. The pits are excavated completely through Unit 2, the most highly fractured tuff unit, thus destroying the fracture system and the likelihood of fracture flow through this unit. Also, to our knowledge, the only observations of fracture transport at LANL occurred beneath a liquid radioactive-waste disposal trench site that was heavily used between 1945 and 1952 (Rogers, 1977). The tuff beneath the site was nearly fully saturated by disposal operations. Although radioactivity has been measured in fractures beneath this former liquid waste site, it appears that transport in the fractures stopped soon after waste disposal ceased, based on observations made in the 1960s and 1970s (Nyhan et al., 1984). Also, numerical studies of fracture flow for the site indicate that flow through fractured tuffs is difficult to maintain in low-saturation, high-capillarity systems (Soll and Birdsell, 1998). Because the site in this study is a solid waste site, significant fracture flow through the unsaturated tuff units is unlikely.

Since we cannot predict whether flow occurs in the matrix or the fractures in the basalt, we conservatively treat the basalts as a system dominated by vertical fracture flow. The basalt is modeled as an equivalent continuum medium made up of both fractures and matrix material (Peters and Klavetter, 1988) (see Table 1). Matrix properties are derived from analogue basalts in Idaho (Bishop, 1991). Fracture properties are chosen, through numerical sensitivity studies, so that no lateral diversion occurs at the top of the basalts in the simulations, even when the flow rate exceeds the matrix saturated hydraulic conductivity. Then, the continuum porosity is set equal to the fracture volume fraction, 10^{-4}, to ensure rapid transport of 1 to 5 years through this unit, hence, forgoing any retardation due to matrix flow or sorption. This treatment of transport through the basalt yields a conservative PA result (e.g., faster groundwater travel times and higher peak doses than actually expected).

In designing the boundary conditions for the predictive models, preliminary simulations investigate how well modeled and observed saturations correspond for various infiltration rates, how appropriate a steady-state infiltration rate is, and the representation of fracture matrix interactions. These are described in the Numerical modeling section of this paper.

3.2. Release of radionuclides

The release of radionuclides from the disposal units is represented by one of two release mechanisms: rapid release or solubility-limited release (Vold and Shuman,

1996). The maximum porewater concentration of each nuclide is calculated based on its inventory, its waste volume and the moisture content in the pits. This concentration is then compared to the nuclide's solubility limit to determine which source-release model is appropriate for each nuclide in each disposal unit. That is, if the maximum porewater concentration exceeds the nuclide's solubility limit, the release concentration is held at the solubility limit until that nuclide's inventory has been exhausted. The contaminant flux (Φ) for a solubility-limited element takes the form

$$\Phi = qC_{sl}/h \, \Sigma_j \, \Sigma_i (f_{ij} V_{ij}),$$

where V_{ij} is the total initial waste volume of nuclide i in waste form j in the disposal unit, q is the Darcy flux through the waste package, C_{sl} is the nuclide solubility limit, and h is the representative height of a waste package, taken to be 1 m (Vold and Shuman, 1996). The fraction f_{ij} is a correction factor related to the molar fraction of the nuclide i (of the same element) from waste form, j. This correction factor was determined to be significant only for uranium, which is solubility limited throughout the site (Vold and Shuman, 1996). Wastes may be solubility limited in some disposal units and rapid release in others, depending on the inventory and volume in the particular disposal unit. For example, much larger quantities of plutonium are disposed of in smaller-volume shafts than in larger-volume pits. As a result, the release of plutonium is solubility limited from the shafts but not from the pits.

If the porewater concentration does not exceed the nuclide's solubility limit, the rapid-release model is used. Nuclides with very large solubility limits, such as ^{129}I and ^{99}Tc, are controlled by this mechanism throughout the site. The contaminant flux for the rapid-release model takes the form

$$\Phi = Q\lambda^2 t e^{-\lambda t},$$

where Q is the total inventory (moles) of the nuclide in the disposal unit, λ is the release constant ($\lambda = q/\theta h$), and θ is the average moisture content of the disposal unit, taken to be 0.08 based on field observations (Vold and Shuman, 1996). The rapid-release source term is highly dependent on the Darcy flux through the waste package (q), which is assumed to equal the percolation rate. This flux dependence is demonstrated in Fig. 6,

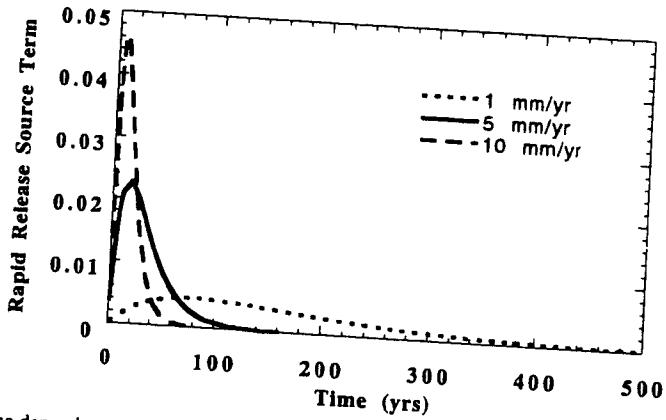

Fig. 6. The dependence of the rapid-release, source-term model [year^{-1}] on the infiltration rate.

which shows the time-dependent behavior of the rapid-release model ($\lambda^2 te^{-\lambda t}$) for different percolation rates. For example, with a percolation rate of 10 mm/year, the rapid-release model predicts that the waste is completely released within the first 80 years, while at a percolation rate of 1 mm/year, complete release from the waste package requires more than 500 years.

3.3. Unsaturated-zone transport processes

The fundamental processes affecting migration rates of solutes in this unsaturated environment are advection, adsorption, diffusion, dispersion, and radioactive decay. A linear-adsorption isotherm (K_d model) is expected to adequately describe adsorption in the unsaturated zone because of the slow percolation rates and the indication that transport in the units above the basalt occurs predominantly in the matrix. Once released from the disposal unit, the nuclide's mobility through the unsaturated zone is controlled by the mesa-top infiltration rate and by the nuclide's K_d and half-life. Thus, the nuclides can be classified by their half-lives and adsorption characteristics. Short-lived nuclides with half-lives less than 20 years, such as ^{3}H and ^{60}Co, are expected to decay to insignificant levels before reaching the aquifer, so they are not considered in the analysis. Nuclides can be grouped as nonsorbing, weakly sorbing, and strongly sorbing, as shown in Table 2. The nonsorbing nuclides ^{14}C, ^{129}I and ^{99}Tc are expected to travel most rapidly, while the strongly sorbing nuclides are expected to have very long travel times. The basalts are assumed to be nonsorbing, consistent with the assumption of rapid transport through this unit.

3.4. Saturated-zone flow and transport processes

Groundwater that percolates from the site through the unsaturated zone is assumed to flow predominantly downward to the main aquifer. Any radionuclides exiting the base of the unsaturated zone enter the saturated zone through the upper boundary. Although an understanding of the geology and groundwater system under LANL is still being developed, Purtymun (1995) suggests that the groundwater in the main aquifer flows in a southeasterly direction to the Rio Grande. Our saturated-zone model is based on this hypothesis. Advection, linear adsorption, diffusion, dispersion, and radioactive decay again control saturated-zone migration of solutes.

4. Numerical model

4.1. Overview

The unsaturated-zone flow and transport model is a three-dimensional representation of the complex mesa/canyon hydrogeologic system. Infiltration is assumed to be steady in time but variable in space over the mesa top and two bordering canyons. The model incorporates the position and inventories of 34 disposal pits and five shaft fields already located at the site along with those of the four proposed expansion pits and shafts. Two

pathways are considered: downward migration through the unsaturated zone to the aquifer, and lateral migration to the mesa sides followed by deposition into the nearby canyons, and subsequent migration through the unsaturated zone to the aquifer. Time- and spatially variable nuclide flux from the unsaturated zone enters the single material, three-dimensional, saturated-zone model, thus maintaining the spatial distribution of nuclide flux exiting the unsaturated zone. The simulations are run for 10,000 years in order to cover the regulatory-driven 1000-year compliance period (Hollis et al., 1997) with a 10,000-year uncertainty analysis.

The simulations are run with FEHM, a two- or three-dimensional finite-element/finite-volume code suitable for simulating systems with complex geometries that arise when modeling subsurface flow and transport (Zyvoloski et al., 1997). In the unsaturated zone, the governing equations for flow are based on the principles of conservation of water and air. Darcy's law is assumed to be valid for the momentum of the air and water phases in the unsaturated zone and for the water phase in the saturated zone. The convection–dispersion equation governs solute transport (Jury et al., 1991; Zyvoloski et al., 1997) in these analyses.

4.2. Computational grid

The stratigraphic configuration used for the unsaturated-zone model is derived from various sources including the LANL site-wide geologic model (Vaniman et al., 1996), well-log picks, and surface observations. The data set is interpolated with the Stratagraphic Geocellular Modeling (SGM) Software (Stratamodel) to generate the three-dimensional geologic framework model shown in Fig. 7, which includes the thinning of the Bandelier tuff units at the eastern end of the site.

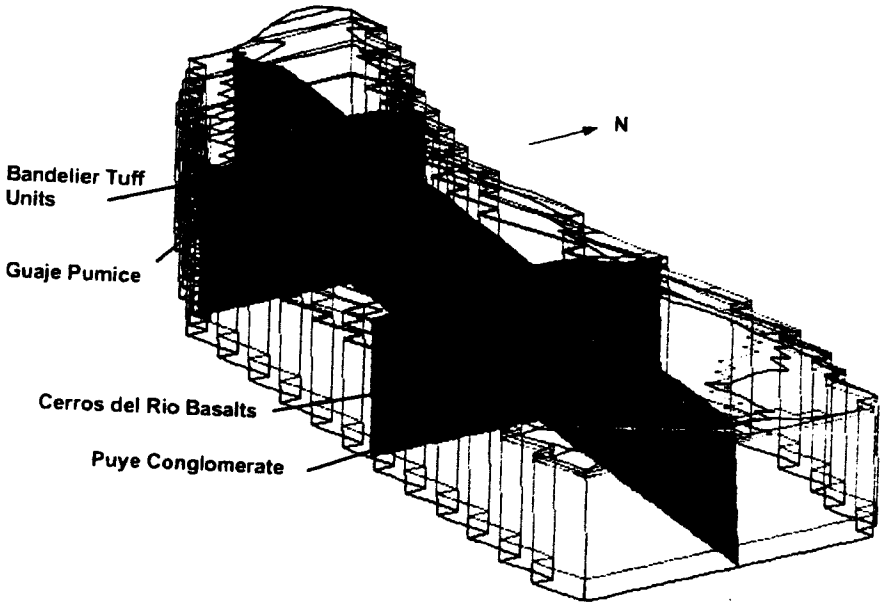

Fig. 7. Three-dimensional, stratigraphic framework model of the site.

The three-dimensional unsaturated-zone grid is generated with the Geomesh/X3D software (Gable et al., 1995) from the geologic framework model. An initial grid is constructed with the 45.7-m spacing of the geologic framework model and then resolved to include the 38 waste disposal pits (Fig. 4) and to better delineate the mesa sides. The final grid contains 41,542 nodes and 254,614 tetrahedral elements. Pit regions are defined by a set of nodes that outline several adjacent pits with internal nodes down the pit centerlines. The volumes associated with these internal nodes approximate true pit volumes. The internal pit nodes are assigned hydrologic properties for crushed tuff (the pit backfill material) and act as the source region for radioactive waste during the transport calculations. Fig. 4 shows the outline of the waste disposal pits, the internal pit nodes, and the outline of the mesa edge.

The saturated-zone model extends from just west of the site to the Rio Grande. The grid is rectangular and oriented perpendicular to groundwater equipotentials. It is 9773 m long, 1280 m wide, and 100 m deep with 19,580 nodes and 102,960 tetrahedral elements. To better model the vertical dispersion of the contaminant plumes entering the aquifer from the unsaturated zone, the vertical element height is refined near the water table. The grid is also refined horizontally beneath the site to approximately 500 m downstream to accurately capture the spatial distribution of the radionuclides as they move toward the downstream compliance regions.

4.3. Boundary conditions

4.3.1. Preliminary calculations

As described in the conceptual model, a series of preliminary calculations was performed to evaluate infiltration rates and modeling assumptions, such as the use of steady flow rates and the dominance of matrix flow through the tuff units.

To determine appropriate infiltration rates for the site, simulated saturation profiles for a number of different steady, mesa-top infiltration rates are compared to site field data. Infiltration rates of 10 mm/year, 1 mm/year, 0.1 mm/year, 0.01 mm/year and 0.0 mm/year were run using the two-dimensional cross section shown in Fig. 3. Fig. 5 shows the calculated steady-state saturation profiles at the center of the mesa for the five infiltration rates along with the ranges of in situ saturation data measured in the six Bandelier Tuff units. The shape of the calculated saturation profiles shows the same trend as the data (e.g. saturations decrease from Unit 2 to Unit 1v-u and then increase again in Unit 1v-c, etc.), but no single infiltration rate yields predicted saturation values that fit the entire data set. Results for the lowest infiltration rates (0.01 and 0.0 mm/year) most closely match the site saturation data in Units 2 and 1v-u, the two mesa-top units. Higher infiltration rates (0.1 and 1 mm/year) are needed to match the saturation data from Units 1v-c and 1g, and an even higher rate (10 mm/year) is needed to match the data in the Cerro Toledo and the Otowi Member. Newman (1996) also found that no single percolation rate fits in situ chloride data from the site. For example, he estimates flux rates within the mesa ranging from 0.03 to 1.5 mm/year and flux rates below the mesa near 5 mm/year based on chloride mass-balance based flux estimates. Based on these two studies, the PA calculations use a range of mesa-top infiltration rates from 1 to 10 mm/year.

Since deep percolation is thought to be seasonal with most occurring during spring snow melt and to a lesser extent during the summer thunderstorm season (Rogers et al., 1997), separate, small-scale modeling studies were performed to test the assumption of steady-state flow used for the PA calculations. Birdsell et al. (1999) studied the effects of annual transients in percolation rate on unsaturated-zone transport at the site. They found that simulated transient pulses are damped with depth so that the calculated cumulative contaminant flux at the base of the Bandelier Tuff is similar under transient and steady flow fields. By using a steady infiltration rate at the high end of the expected range, and forcing short travel times through the basalt, the subsequent transport calculations are expected to yield conservative results, assuming that fracture flow has little effect on transport in the upper two fractured tuff units.

Numerical studies of fracture flow for the site indicate that transport through fractured tuffs has a minimal effect on contaminant flux at depth (Soll and Birdsell, 1998). Also, during pit emplacement, the uppermost unit (Unit 2) and often part of Unit 1v-u are excavated, thus destroying the natural fracture network in the area surrounding the waste. Because of these factors, fractures are considered only for the deep basalt in the unsaturated-zone model.

4.3.2. Performance calculations

The mesa/canyon setting leads to a set of spatially dependent, surface boundary conditions categorized by position depending on whether infiltration is applied to the mesa top, to the relatively wet Pajarito Canyon, or to the dry Cañada del Buey, as shown in Fig. 3. Evaporative nodes along the mesa sides are held at a fixed saturation of 0.03, which is equivalent to an ambient relative humidity near 50%.

Five different unsaturated-zone flow fields are considered in order to study the sensitivity of the simulated results to infiltration rate. Three mesa-top flows are used (1, 5 and 10 mm/year), two flow rates for Cañada del Buey are considered (1 and 5 mm/year), and three flow rates for Pajarito Canyon are used (20, 50 and 100 mm/year). Table 3 summarizes the five cases. The base case, 5_1_50, is thought to be conservative for the site based on Newman's (1996) chloride flux estimates and on the saturation profiles shown in Fig. 5, which show that the range 1 to 10 mm/year fits the higher range of site moisture data. No-flow boundary conditions are applied to the sides of the unsaturated-zone grid. The bottom boundary represents the water table, where both water and radionuclides can exit.

Table 3
Infiltration rates (mm/year) used as upper boundary conditions

	Mesa Top	Cañada del Buey	Pajarito Canyon
1_1_20 (lowest flow case)	1	1	20
5_1_20	5	1	20
5_1_50 (base case)	5	1	50
10_1_20	10	1	20
10_5_100 (highest flow case)	10	5	100

A steady flow field is calculated for the saturated-zone model by applying a pressure head difference of 101 m (Purtymun, 1995) across the east and west sides of the model. No-flow boundaries are used for the top, bottom, north and south sides. Recharge is believed to occur mainly to the west of the site, at higher elevations in the Jemez Mountains. A water-balance estimate shows that the volume of water entering the aquifer from the unsaturated zone at the site is negligible compared to the aquifer volume (Birdsell et al., 1999). Thus, water flowing from the unsaturated zone to the aquifer is not included.

Simulated time-dependent radionuclide flux exiting the base of the unsaturated zone is recorded at each time step and used as the radionuclide source term for the saturated zone. To supply an adequate spatial distribution, the bottom boundary of the unsaturated-zone grid is divided into 28 regions for which nuclide flux is reported. Then, nodes corresponding to these 28 regions are defined as source regions for the saturated-zone model to retain the spatial distribution of plumes that have migrated through the unsaturated zone from the original disposal units.

4.4. Source term

The source-release models used to calculate the time-dependent nuclide release rate from each disposal unit (Vold and Shuman, 1996) are incorporated directly into FEHM (Zyvoloski et al., 1997) and include both rapid release and solubility-limited release. Because wastes from the four disposal-unit classes are governed by different regulations (Hollis et al., 1997), the transport of each waste class is simulated separately. These simulations can determine the impact of an individual waste class or can be combined by superposition to determine the impact of the total inventory. Also, by differentiating the impact of the individual waste classes, the calculations can help define waste acceptance criteria for future wastes or a part of the analysis can be updated if inventory corrections are required.

The extrapolated total inventories for the 1957–1970 and 1996–2044 wastes (Shuman, 1997a) represent the estimated and projected values, respectively. Because the distribution of waste among the individual disposal units within these two waste classes is not characterized, their inventories are uniformly distributed between all of the pit or shaft nodes for the particular waste class. However, inventory and waste volume are known in greater detail for the 1971–1988 and for the 1988–1995 wastes. For each nuclide in these two waste classes, the total inventory and waste volume are available for each pit and shaft field and are therefore distributed appropriately between the finite-element model nodes at the source locations.

4.5. Dose

The saturated-zone radionuclide concentrations are converted to two types of doses to humans: the groundwater dose which results from the direct ingestion of groundwater extracted from the regional aquifer, and the groundwater component of the all-pathways dose which results from ingestion of groundwater and of foodstuffs raised with contaminated water. The dose conversion factors shown in Table 4 are used to convert

Table 4
Factors for converting aquifer concentration to dose

Nuclide	Conversion from mol/l to Ci/m^3	Conversion from Ci/m^3 to mrem/year for the drinking water pathway dose	Conversion from Ci/m^3 to mrem/year for the all pathways dose
^{14}C	6.24×10^{4}	1.53×10^{6}	4.11×10^{6}
^{99}Tc	1.686×10^{3}	9.49×10^{5}	3.04×10^{6}
^{129}I	21.03	2.04×10^{8}	2.70×10^{8}

aquifer concentrations to nuclide-specific doses. These factors are a function of the nuclide half-life and the consumption rates of water, food and soils (Shuman, 1997b). The total dose is the sum of the nuclide-specific doses. Once the total dose is calculated for each location in the aquifer, the maximum dose is reported along a compliance boundary 100-m downgradient from the site fence line (Fig. 4) as required by DOE regulations (Hollis et al., 1998) and also for an individual living in Pajarito Canyon. The dose at the downgradient compliance point results from waste that migrates downward from the disposal units through the unsaturated zone to the aquifer. The dose in Pajarito Canyon results from waste that migrates laterally to the mesa sides, is deposited into the canyon, and then migrates to the aquifer. The groundwater doses are not only reported by their location and pathway (e.g., groundwater vs. all pathways), but doses are also reported by their original waste classification (PA or CA), as described in the source term discussion.

5. Results

5.1. Unsaturated-zone transport

5.1.1. Screening

Unsaturated-zone transport calculations were run for ^{14}C, ^{129}I, ^{237}Np, ^{99}Tc,and ^{238}U using the base-case, steady flow field, 5_1_50 (Table 3). These nuclides were chosen because of their low distribution coefficients, ranging from 0 to 2.43 for most of the unsaturated-zone units. Only ^{14}C, ^{129}I, and ^{99}Tc, the nonsorbing nuclides, show any breakthrough to either the water table or the mesa side over the 10,000-year time frame. Thus, we are able to eliminate the remaining nuclides from consideration in the dose assessment because their distribution coefficients are larger than those of ^{237}Np and ^{238}U, which did not break through. This screening includes the consideration of all daughter products in the radionuclide decay chains, all of which have K_d values larger than those of ^{237}Np and ^{238}U. Calculations of ^{237}Np and ^{238}U transport using the highest flow rates, 10_5_100, also indicate no breakthrough, thus showing that this screening technique applies for all flow fields considered in this study.

This screening technique does not consider colloid-facilitated radionuclide transport. Although colloid-facilitated transport has recently been implicated with trace amounts of

plutonium in the saturated zone at the Underground Test Area of the Nevada Test Site (NTS) (Kersting et al., 1999); there are several key differences between the NTS and LANL systems. Unlike the NTS, where radionuclides are emplaced in the fractured, saturated-zone flow path, the source at LANL is in the unsaturated zone where fracture flow in most units is expected to be negligible. Whereas mobile colloids are abundant in saturated systems (DeGueldre et al., 1997), colloids are less likely to be mobile in matrix-flow dominated unsaturated systems (Wan and Wilson, 1994). Low mobile colloid concentration, filtration due to size exclusion in pores, and retardation at air–water interfaces reduce the likelihood of colloids playing a significant role in enhancing migration of otherwise immobile radionuclides in the LANL system.

The screening technique used above is dependent on the 10,000-year uncertainty period. We have also developed another more general screening technique that is independent of the compliance period (Birdsell et al., 1995). The technique compares the nuclide's half-life to its unsaturated-zone travel time. Generic breakthrough curves are calculated for various K_d values to estimate a functional form for the time of first arrival (estimated in our case as 0.1% of the peak concentration) vs. K_d. In 20 half-lives a waste decays to 10^{-6} times its original inventory. Thus, if a nuclide's unsaturated-zone travel time is greater than 20 times its half-life, there is essentially no release to the aquifer, and the nuclide requires no further consideration unless it has long-lived daughters. This comparison provides a generic method to eliminate transport calculations for programs having no regulatory compliance period, such as the Swedish, Swiss and U.K. high-level waste programs (Thompson, 1999). In a previous study of the LANL site that considered peak doses over hundreds of thousands of years, over half the nuclides were eliminated from further consideration with this method (Birdsell et al., 1995). This screening technique can also be extended to any waste that exponentially degrades, including biodegradable wastes. Note that for extremely large inventories; a reduction of 10^{-6} times the initial inventory may still produce an unacceptable dose. In such a case, the analyst should compare the travel time to the appropriate larger number of half-lives to achieve an acceptable reduction factor.

5.1.2. Transport calculations

5.1.2.1. Base-case flow field. Fig. 8a–d shows the simulated ^{129}I plumes in the unsaturated zone for the four age-dependent waste classes (Fig. 4) after 1000 years using the base-case flow field. Although the infiltration rate at each source region is the same (5 mm/year), the four plumes are quite different due to both inventory variations and differences in bed thickness. The inventory distribution in the disposal units is heterogeneous, leading to large variations in radionuclide flux from the disposal units to the unsaturated zone. For example, the 1971–1988 (Fig. 8b) inventory dominates the total site release of ^{129}I to the aquifer at 1000 years. Also, the 1988–1995 shafts located near the southern edge of the mesa (left side of Fig. 8c) concentrate nearly 80% of the 1988–1995 ^{129}I inventory into a small area. This localized inventory produces a predominant plume at the southern portion of the mesa, while the pits to the north and west produce the less concentrated plumes. The location of the basalt unit and the effect of the vertical, fracture-dominated flow through this unit on plume migration is readily

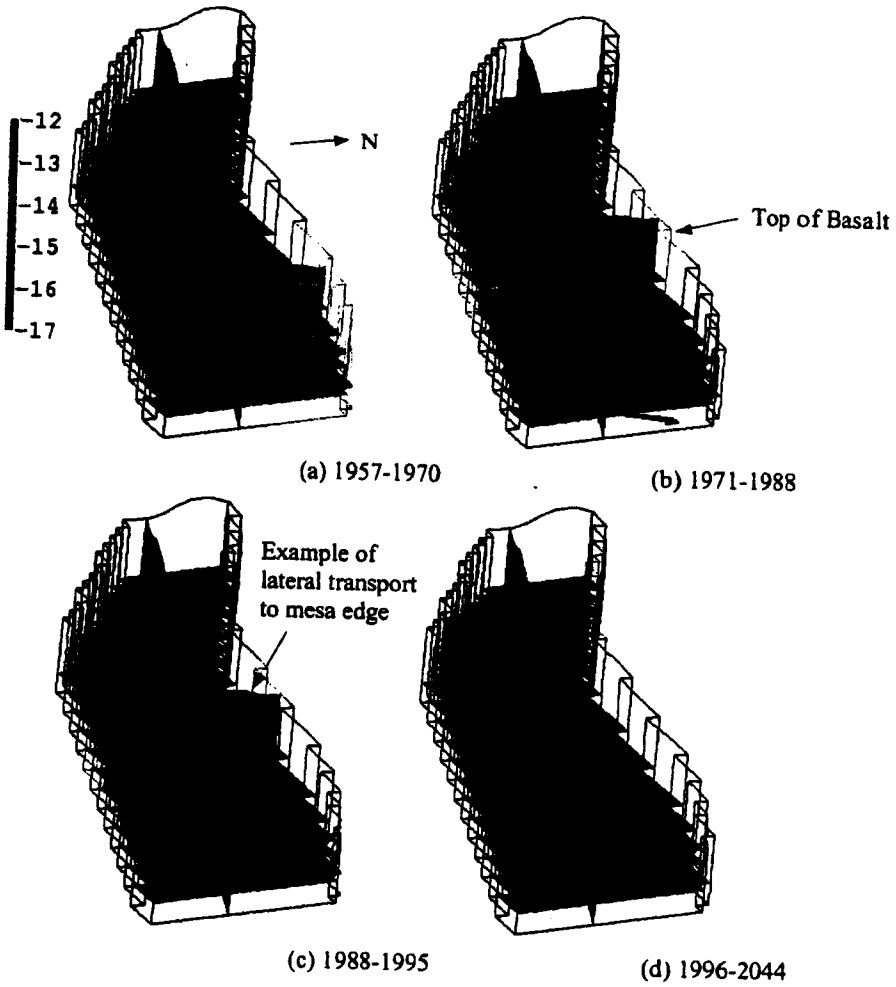

Fig. 8. ^{129}I plumes (log concentration, mol/l) in the unsaturated zone at 1000 years for the four different source regions, base-case flow field.

visible in these figures. We see that once the solutes reach the basalt, they migrate quickly through the unit. In the 1996–2044 waste scenario (Fig. 8d), only the plume's leading edge reaches the basalt after 1000 years because the Bandelier Tuff units are much thicker beneath this proposed expansion area.

Fig. 9 shows the total time-dependent flux of ^{129}I from the unsaturated zone to the saturated zone for the four waste classes (Fig. 4) using the base-case, steady flow field. This figure also demonstrates the dominance of the larger 1971–1988 inventory on ^{129}I releases from the site. The release of this nuclide is controlled by the exponential, rapid-release model, which produces flux-vs.-time curves that peak in less than 10,000 years.

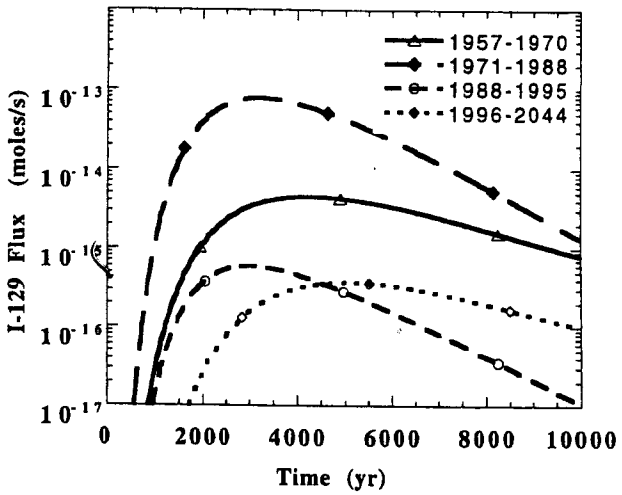

Fig. 9. Total flux of ^{129}I from the unsaturated zone to the saturated zone from the four source regions, base-case flow field (5_1_50).

For each of the nuclides and the four waste classes, the solute flux is increasing at 1000 years causing the compliance-period peak dose to occur at 1000 years. Fig. 9 shows that during the 1000-year to 10,000-year uncertainty period, the four ^{129}I curves peak at different times. The other two nuclides also show a distribution for the occurrence of the peak solute flux. Because of these distributions in time, a formal dose calculation is required to predict when the peak dose for the uncertainty period occurs.

5.1.2.2. Other flow fields. To assess the effect of uncertainty in flow rate on transport results, we examine the transport of the 1988–1995 ^{129}I inventory using different flow fields and compare the nuclide fluxes through the unsaturated zone. Fig. 10 shows the total flux of ^{129}I for the five flow fields described in Table 3. By comparing the 1_1_20 case, the 5_1_20 case, and the 10_1_20 case, we see that increased mesa percolation leads to faster breakthrough and increased solute flux through the unsaturated zone. This flow-rate dependency is compounded by the velocity-dependent rapid-release source term (Fig. 6). The solute flux at 1000 years for the lowest flow case, 1_1_20, is five to seven orders of magnitude less than the other cases considered. This case is used to predict the lower-bound dose in the uncertainty analysis. By comparing the 5_1_20 case to the 5_1_50 case, we see that additional flow through Pajarito Canyon results in faster breakthrough and increased solute flux to the saturated zone. The 10_5_100 case represents the wettest case and yields the fastest breakthrough and highest flux to the saturated zone and, consequently, the highest dose over the first 1000 years. This case is used to estimate an upper-bound dose for the uncertainty analysis.

The first arrival (0.1% of peak) of ^{129}I at the water table varies significantly for the different flow scenarios, as shown in Fig. 10. For the base-case calculations, the time of first arrival is about 600 years. Whereas the first arrival for the highest flow case is half

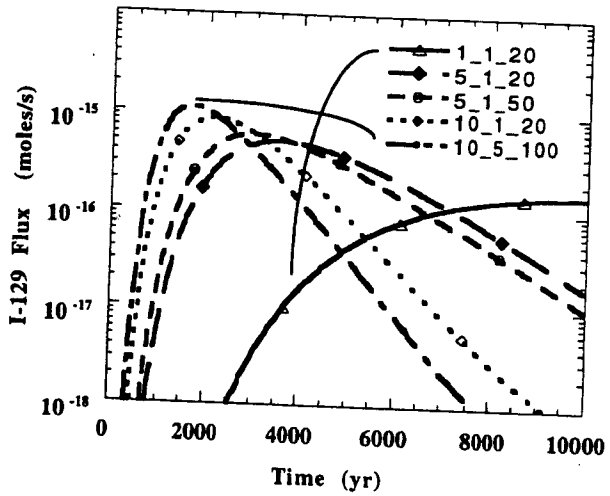

Fig. 10. Total flux of the 1988–1995 ^{129}I inventory from the unsaturated zone to the saturated zone for various flow cases.

the 600 years of the base case, the lowest flow case's first arrival is at 2000 years, well beyond the 1000-year compliance period.

5.1.2.3. Transport toward the mesa sides. Flux of nuclides toward the mesa sides is observed in the simulations (Fig. 8), so the impact of this pathway on the dose is assessed. As in the case of downward transport, only the three nonsorbing nuclides ^{14}C, ^{129}I and ^{99}Tc are of concern over 10,000 years. To summarize, our analysis of this pathway takes several steps. First, the transport of nuclides through the unsaturated zone is simulated, yielding the nuclide flux to the two mesa sides. Next, we conservatively assume that the radionuclide flux through the mesa sides is immediately available for transport from either Pajarito Canyon or Cañada del Buey, where their continued migration to the aquifer is simulated. Those contaminants reaching Pajarito Canyon lead to the highest aquifer-related doses because of the higher percolation rate in Pajarito Canyon. Therefore, we simulate transport from the floor of the Pajarito Canyon through the unsaturated zone to analyze the potential dose for this pathway, including three canyon percolation rates for the uncertainty analysis. The final step in the analysis of this pathway involves calculating the concentration of the contaminants in the saturated zone beneath Pajarito Canyon, starting with the nuclide flux from the unsaturated zone. The receptor for this pathway lives in the canyon and uses water from a well drilled through the canyon floor to the aquifer.

The simulated aquifer-related dose resulting from lateral transport to the mesa sides is expected to be orders of magnitude higher than the true dose that might occur from this pathway for two reasons. First, the simulated lateral transport of the nuclides occurs because of the very low, fixed-saturation boundary condition along the mesa sides. This boundary condition causes a strong lateral pressure gradient that pulls water and subsequently nuclides from the mesa interior toward the sides. However, if drying really

occurs throughout the mesa top, in fractures and along surge beds rather than only at the mesa exterior, the resulting pressure gradient would decrease. This decreased driving force would lead to localized contaminant movement (on the order of the fracture spacing) toward the mesa sides and toward fractures, which would significantly lower doses from this pathway.

Second, the flux is calculated as though the nuclides are immediately available for subsurface transport through the canyon bottoms once they reach the mesa edge, perhaps via surface runoff. However, because nuclides are heavy and nonvolatile, they actually accumulate along the evaporation sites rather than exiting the tuff matrix. Longmire et al. (1996) have observed elevated chloride, sulfate, and sodium concentrations in porewaters extracted from unsaturated-zone Bandelier tuff samples, which suggest that evaporation leads to the concentration of dissolved species. Newman's (1996) data showing elevated chloride and stable isotope concentrations also support this interpretation.

5.2. *Saturated-zone transport*

With the transient unsaturated-zone nuclide flux as the saturated-zone source term, advective–dispersive–reactive transport is simulated to locations downstream of the site boundary for the direct, downward pathway. Fig. 11 shows the concentration profiles at two locations in the saturated zone for the 1988–1995 ^{129}I inventory. The locations represent the point of maximum dose for the 1988–1995 waste and the compliance point, which is 100 m downstream from the site fence line, but approximately 800 m from the 1988–1995 pits (Fig. 4). Such concentration information, along with analogous information for the other waste classes and the other two nuclides, is used in the formal dose assessment (Shuman, 1997b). The two curves have the same shape with dilution

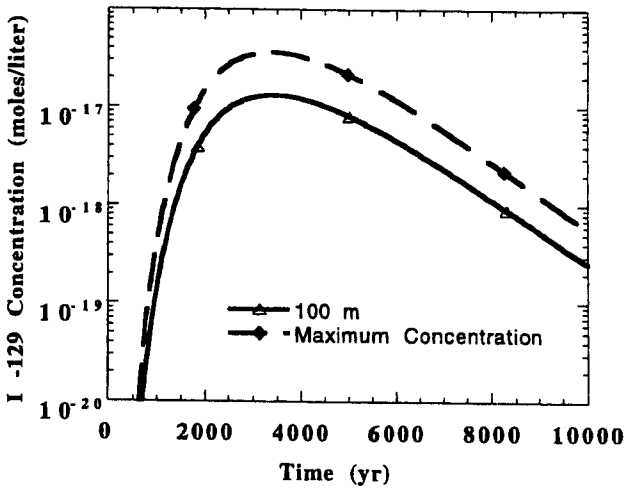

Fig. 11. Concentrations in the saturated zone for the 1988–1995 ^{129}I inventory at the point of maximum concentration and at the 100-m compliance point with the base-case, unsaturated-zone flow field.

and mixing decreasing concentration by a factor of about three at the 100-m distance. Dilution at the 100-m compliance point increases with distance from the original waste site (i.e. aquifer dilution for the 1996–2044 waste is greater at the 100-m compliance point than for the 1957–1970 waste). The concentration profiles also mimic the unsaturated-zone contaminant flux curve shown in Fig. 9. Using the current estimated dispersion coefficients, aquifer dilution of unsaturated-zone concentrations is approximately a factor of 500 between the maximum concentration exiting the unsaturated zone and the aquifer concentration at the 100-m compliance point. The simulated plumes disperse throughout the 100-m depth of the model soon after entering the aquifer based on the chosen transport parameters. Therefore, concentration profiles at the 100-m compliance point are nearly uniform with depth with the highest concentration at the top of the water table. This high dilution factor is evaluated later in the uncertainty analysis.

5.2.1. Dose assessment

The dose conversion factors shown in Table 4 are applied to the three-dimensional ^{14}C, ^{129}I, and ^{99}Tc saturated-zone concentration fields to obtain dose fields. These dose fields are then summed to obtain the total groundwater dose and the groundwater component of the all-pathways dose for the entire PA inventory (1988–1995 plus 1996–2044 waste) and the Composite Analysis inventory (all wastes). The 100-m compliance points are then identified as the locations of maximum dose at distances 100 m from the site fenceline for the PA and CA wastes.

The DOE performance objectives are compared to the calculated maximum dose values in Table 5 for nuclides that have traveled continuously downward through the unsaturated zone. The comparison is shown for the base-case flow field, the highest-flow field, and the lowest-flow field at 1000 years. Also compared are the peak doses during the 10,000-year uncertainty period for the base case. All doses calculated for this pathway are six or more orders of magnitude lower than the performance objectives. For the lowest-flow case, doses are negligible because over 99% of the inventory for the nonsorbing radionuclides remains in the unsaturated zone.

The dose assessment for the total system, including other pathways, is presented by Shuman (1997b). Shuman calculated a higher dose during the first 1000 years for waste transported laterally to the mesa side than for waste that follows the continuous downward path to the water table. The receptors are different for these two cases: for

Table 5
Maximum groundwater and all-pathways doses for the PA and CA wastes (millirem/year)

	PA — ground water	PA — all pathways	CA — all pathways
Performance objective	4	25	100
1000 years (base case)	2.4×10^{-7}	6.5×10^{-7}	3.7×10^{-5}
Peak dose (base case)	3×10^{-5}	1×10^{-4}	2×10^{-3}
	@ ~4500 years	@ ~4500 years	@ ~3000 years
1000 years (highest flow)	8.0×10^{-6}	2.2×10^{-5}	1.4×10^{-3}
1000 years (lowest flow)	9×10^{-12}	2×10^{-11}	1×10^{-10}

waste that is transported laterally, the receptor lives in Pajarito Canyon, while for the downward pathway, the receptor lives at the 100-m compliance point. The earlier arrival time and higher aquifer concentrations for the lateral pathway are caused by the assumption of immediate release into Pajarito Canyon and the fast canyon recharge rate. For example, the peak aquifer dose for the base-case, unsaturated-zone flow field caused by migration toward the mesa side and subsequent deposition into Pajarito Canyon occurs after 800 years. The PA groundwater dose is 4.5×10^{-5} and the PA all-pathways dose is 1.3×10^{-4}. These doses are higher than those reported in Table 5, but still five to six orders of magnitude lower than the performance objectives.

We expect that the simulated lateral pathway is overestimated, for reasons discussed previously. To assess the impact of overestimating this pathway, a few simulations were rerun with the evaporative boundary condition along the mesa sides replaced by a no-flow boundary condition. The simulations show that the boundary condition imposed on the mesa side has a strong effect on the simulated migration path. With an evaporative driving force, much of the waste is pulled laterally toward the mesa sides before diverting downward. This increases the distance that the waste travels through the unsaturated-zone and delays breakthrough to the aquifer. With the no-flow boundary condition, the dose resulting from continuous downward migration through the unsaturated zone increases while the dose due to the lateral pathway disappears. For example, the 1000-year doses for the downward pathway increase by roughly a factor of 100 to 1000 because the breakthrough curves advance in time. However, the peak dose increases by only a factor of about 50. These values are still much lower than the performance objectives (Table 5).

6. Uncertainty

As in any predictions of the long-term migration of solutes through the subsurface, the results of these transport simulations contain intrinsic uncertainty. Here we summarize what we believe are the more important uncertainties and discuss their impact. The greatest uncertainties associated with predicting aquifer-related doses from the site are related to our understanding of the mechanisms that control flow and transport within the unsaturated zone and our ability to model these mechanisms. At this point, we feel that uncertainty related to the hydrologic processes themselves (conceptual model uncertainty) dominates our ability to make accurate predictions of transport at the site more so than uncertainty related to the hydrologic and geochemical properties (data uncertainty). However, predicted doses using parameters from the most conservative ends of the uncertain ranges are still well below those that would cause concern.

6.1. Unsaturated-zone flow

In situ saturation data are difficult to match with any single infiltration rate using our current unsaturated-zone model. It is possible that the mesa and the submesa units are not strongly connected hydrologic systems. Higher saturations beneath the mesa may result from a recharge source other than percolation through the mesa or could represent

moisture from a past, wetter climate. Evaporation is clearly an important mechanism controlling flux rates within the mesa, yet it is only indirectly incorporated into the flow modeling through the application of low infiltration rates of 1 to 10 mm/year and the evaporative boundary conditions along the mesa sides. By directly simulating evaporation in fractures and surge beds within the mesa interior, calculated solute migration through the mesa may behave similarly to that seen with environmental tracers such as chloride. These tracers accumulate within the mesa and have estimated travel times on the order of 1000 to 17,000 years through the Bandelier Tuff (Newman, 1996). Accumulation of nuclides within the mesa top would lead to a reduction in predicted aquifer-related doses.

The mesa-top infiltration rate has the greatest impact on the simulated migration of waste through the unsaturated zone. It controls both the source release rate and subsequent downward solute migration. We bounded this uncertainty by considering a base-case flow field and high- and low-flow cases. As shown in Table 5, a variation in mesa-top infiltration rate from 1 to 10 mm/year results in a range of six orders of magnitude in the 1000-year groundwater-related doses. Clearly, a good understanding of this key parameter is important to the dose assessment. However, because doses are so much less than the performance objectives, conservative yet realistic infiltration rates seem adequate for this site.

Other uncertainties are related to flow within the deeper unsaturated-zone units for which few hydrologic data are available. The simulations take virtually no credit for transport times through the Cerros del Rio Basalts, which make up more than 50% of the unsaturated zone. Understanding the mechanisms that govern flow and transport in the deeper unsaturated-zone and incorporating them into the model could add hundreds or thousands of years to predicted transport times and result in lower peak aquifer concentrations.

The transport results are based on the steady-flow assumption and on the use of matrix, hydrologic properties for all tuff units at the site. Our understanding of the response of this fractured system to transient flow events remains uncertain. Transient calculations (Birdsell et al., 1999) indicate that the steady-flow assumption is adequate because fluctuations in both saturation and contaminant flux rates dampen with depth even when including fractures in the upper two units. Fracture infiltration studies (Soll and Birdsell, 1998) lead us to the conclusion that fracture flow is difficult to initiate and is short lived in the upper two tuff units at the observed low field saturations. This conclusion helps justify the use of the matrix hydrologic properties for the calculations. We should note that only Unit 2 and the uppermost portion of Unit 1v-u show evidence of significant fracturing (Krier et al., 1997), and that these are excavated during disposal operations. Therefore, the waste should not migrate through any highly fractured units until reaching the basalts. The matrix units that underlie the disposal units should attenuate transient pulses and fracture flow should be minimal, except in the basalts. Although we are confident in the assumptions made here, this hypothesis could be tested by verifying the absence of young environmental isotopes such as bomb-pulse ^{36}Cl at depth.

Although there is variability in hydrologic properties at the site, mean values were chosen for the properties used in the modeling. A sensitivity analysis using the minimum

and maximum reported saturated hydraulic conductivity values for the tuff units (Birdsell et al., 1999) showed variations in unsaturated-zone travel times of approximately ±25% from the mean. With higher conductivity values, the flux-vs.-time curves shown in Fig. 9 move to the left, and predicted doses increase. This shift could potentially elevate doses by about two orders of magnitude, still well below the performance objectives. Heterogeneity in hydrologic properties could lead to preferential flow paths through the unsaturated zone that could produce shorter travel times and regions of higher flux. The effects of heterogeneity are discussed later.

6.2. Saturated-zone flow

While it is probably heterogeneous in nature, the saturated zone is modeled as a single, homogeneous, isotropic medium. Heterogeneity can lead to preferential flow paths that may yield higher aquifer concentrations. Aquifer concentrations are, however, limited by the flux of nuclides through the unsaturated zone and even the maximum calculated aquifer doses, before any migration occurs in the aquifer, are six orders of magnitude less than acceptable limits.

The aquifer velocity may be double that used here (Purtymun, 1995), which would move the plume more quickly toward the compliance point and possibly dilute the plume. This effect is small because the travel time through the aquifer is short compared to that through the unsaturated zone. One other uncertainty is related to the modeled aquifer depth. The plume disperses throughout the entire modeled depth of 100 m. Had the modeled depth been greater, the plume would have dispersed even further with a corresponding decrease in concentration.

6.3. Transport properties

The transport simulations are highly sensitive to the value of the distribution coefficient, K_d, in the unsaturated zone. Uncertainty in this parameter for weakly sorbing nuclides plays an important role in the results of this analysis. According to our simulations, a nuclide with a K_d greater than 2.5 will not reach the saturated zone within 10,000 years. Previous simulations (Birdsell et al., 1995) indicate that a K_d as low at 0.3 will retard nuclides sufficiently to prevent breakthrough to the aquifer within 1000 years. Site-specific K_d values for several nuclides with large inventories and expected low distribution coefficients were measured to decrease the uncertainty in the model predictions that results from data uncertainty related to retardation (Longmire et al., 1996). The combination of a low-K_d nuclide traveling along a fast flow path could lead to breakthrough of nuclides other than the three nonsorbing species found to be of concern. However, for this mechanism to be significant to the dose assessment, fast flow paths would need to contact a significant portion of the inventory. The effect of inventory uncertainty can be estimated by linearly scaling the simulation results.

In the saturated-zone model, longitudinal and transverse dispersivity values of 20 and 2 m, respectively, are used. Larger dispersivity values are justifiable based on the distance of the pits to the 100-m compliance point. For example, the 1996–2044 pits are

on the order of 1300 m from the compliance point, which leads to longitudinal and transverse dispersivity values of 130 and 13 m, respectively, based on Neuman's (1990) empirical fit to field data. Longitudinal and transverse dispersivity values of 1 and 0.1 m are used for the unsaturated-zone modeling, and again, higher values may be warranted. The effect of increasing the dispersivity in either case is that an increased longitudinal dispersivity results in a faster arrival time for the plume's leading edge. An increase in the transverse dispersivity leads to a lower peak concentration.

Sensitivity studies using both higher and lower dispersivity values show that calculated doses do not increase above the maximum doses during the uncertainty period (Table 5).

7. Discussion and conclusions

Numerical simulations are used to predict the long-term migration of radionuclides for the performance assessment of a low-level radioactive waste disposal facility. This case study describes the use of detailed, deterministic process-based models rather than higher-level PA models to perform the ground-water transport calculations required to predict aquifer-related doses. The study first requires knowledge of the site geology, hydrology, and geochemistry, which is used to define the conceptual model of the flow and transport processes that occur at the site. The conceptual model is then described using processed-based numerical models that simulate groundwater flow, radionuclide transport, and dose. The predictions simulate source releases followed by subsequent transport through the unsaturated and saturated zones. The domains are simulated separately but linked through the application of the unsaturated-zone contaminant flux as a boundary condition to the saturated-zone model. A range of unsaturated-zone flow rates is simulated in order to address the effect of uncertainty in infiltration rate on aquifer concentrations. This process-based method is applicable to other low-level waste sites and may provide a more science-based, defensible argument for the acceptance of a PA than more traditional performance-assessment models.

Screening and scaling techniques as well as simplifying assumptions can be used to make a full site assessment tractable. The screening and scaling techniques listed below (items 1 through 3) are applicable to any site. The simplifying assumptions (items 4 and 5) are site specific but serve to illustrate the use of scoping calculations to define the importance of including processes and/or analyses in the study.

(1) Calculations for the LANL site show only the three nonsorbing nuclides ^{14}C, ^{129}I, and ^{99}Tc reaching the aquifer during the 1000-year compliance period or the 10,000-year uncertainty period. Therefore, no formal transport calculations are required for the remaining nuclides in the inventory. With this simple screening technique, the compliance period is compared to the travel times for nuclides with increasing sorption coefficients. Once a cut-off K_d value is found, nuclides with larger K_d values need not be considered.

(2) For longer or unspecified compliance periods a more general screening technique is applied. Generic breakthrough curves are used to estimate travel time as a function of

K_d. Then each radionuclide's half-life is compared to its predicted travel time. If several half-lives (20 is very conservative) are less than the travel time, the nuclide will decay sufficiently so that no release is predicted and an assessment for that species is not necessary. Daughter products must also be considered.

(3) The spatial variability of the source term is important for the case presented in this paper. At other sites, spatial source term information may be unavailable or unimportant. For such sites, generic breakthrough curves developed for the screening can be scaled (with a correction for radioactive decay) based on the inventory of any nuclides still requiring full assessment.

(4) Although the site conceptual model indicates that transients and fracture flow may affect transport through the unsaturated zone, a steady-flow, matrix-dominated model is abstracted for the PA calculations. Preliminary simulations, which indicate that transients are damped with depth (Birdsell et al., 1999) and that fracture flow in the upper units is difficult to maintain (Soll and Birdsell, 1998), justify this abstraction.

(5) A formal uncertainty analysis is not necessary for this case study because simulated doses, calculated through a series of deterministic sensitivity runs, are several orders of magnitude lower than performance measures. The informal arguments concerning the uncertainty of the simulations indicate that the site will remain in compliance even if these factors are taken into account. A probabilistic uncertainty analysis may be required only if predicted doses approach regulatory limits.

Process-based predictions provide a science-based site assessment that readily demonstrates the incorporation of the conceptual model into the numerical predictions. Such predictions can also highlight data needs or identify data that are not crucial to the PA. For this example, the mesa-top infiltration rate is the strongest control over the predicted dose. Chloride profiles (Newman, 1996) and predicted saturation profiles indicate that the range of infiltration rates we have chosen is conservative for the site. However, we are unable to match field data with the steady-flow, uniform infiltration, unsaturated-zone model. If infiltration is spatially variable or transient, the site's performance could be less robust than indicated by our study. For this reason, a continued effort that couples chloride and isotope analyses with modeling studies is planned to better understand local and site-wide net infiltration.

In contrast, although we have little knowledge of the hydrologic properties of the basalt unit at the site, we feel that such data are not currently required. The site appears to perform significantly better than is required despite our assumption of nearly instantaneous transport through the basalt unit. Any data gathered to increase our understanding of transport through the basalt would increase travel times and decrease predicted aquifer concentrations.

The success of the groundwater flow and contaminant transport model described in this paper is demonstrated by the approval of the PA. Having undergone and passed the technical and regulatory reviews required by the DOE for PA approval, the modeling approach and the model were determined to be appropriate for characterizing groundwater risks at numerous formerly used disposal sites undergoing corrective action by the LANL Environmental Restoration Project. This application of a proven site-specific model is expected to save millions of dollars in streamlining the corrective action process at the LANL.

Acknowledgements

This work was conducted under the U.S. Department of Energy, Waste Management Programs. The authors wish to thank B. Robinson, R. Shuman, D. Rogers, E. Vold and B. Newman for technical discussions during this work, and G. Valentine, D. Krier and J. Tauxe for their technical reviews.

References

Birdsell, K.H., Soll, W.E., Bower, K.M., Wolfsberg, A.V., Orr, T., Cherry, T.A., 1999. Simulations of Groundwater Flow and Radionuclide Transport in the Vadose and Saturated Zones Beneath Area G. Los Alamos National Laboratory, Los Alamos National Laboratory manuscript LA-13299-MS.

Birdsell, K.H., Soll, W.E., Rosenberg, N.D., Robinson, B.A., 1995. Numerical Modeling of Unsaturated Groundwater Flow and Radionuclide Transport at MDA G. Los Alamos National Laboratory document LA-UR-95-2735.

Bishop, C.W., 1991. Hydrologic Properties of Vesicular Basalt. Masters thesis, University of Arizona.

Bowen, B.M., 1990. Los Alamos Climatology. Los Alamos National Laboratory Manuscript LA-MS-11735.

Carsel, R.F., Parrish, R.S., 1988. Developing joint probability distributions of soil water retention characteristics. Water Resour. Res. 24, 755–769.

Conca, J.L., Wright, J., 1992. Diffusion and flow in gravel, soil, and whole rock. Appl. Hydrogeol. 1 (1), 5–24.

Degueldre, C., Triay, I., Kim, J., Vilks, P., Laaksoharju, M., Mielkeley, N., 1997. Groundwater colloid properties: a global approach. Environ. Sci. Technol., Submitted.

Eisenberg, N.A., Lee, M.P., McCartin, T.J., McConnell, K.I., Thaggard, M., Campbell, A.C., 1999. Development of a performance assessment capability in the waste management programs of the U.S. Nuclear Regulatory Commission. Risk Anal. 19 (5), 847–876.

Fisher, R.V., 1979. Models for pyroclastic surges and pyroclastic flows. J. Volcanol. Geotherm. Res. 6, 305–318.

Gable, C.W., Cherry, T., Trease, H., Zyvoloski, G.A., 1995. GEOMESH Grid Generation. Los Alamos National Laboratory document LA-UR-95-4143.

Gardner, J.N., Goff, F., Garcia, F.S., Hagan, R.C., 1986. Stratigraphic relations and lithologic variations in the Jemez volcanic field, New Mexico. J. Geophys. Res. 91, 1763–1778.

Gelhar, L.W., Welty, C., Rehfeldt, K.T., 1992. A critical review of data on field scale dispersion in aquifers. Water Resour. Res. 28, 1955–1974.

Hollis, D., Vold, E., Shuman, R., Birdsell, K., Bower, K., Hansen, W., Krier, D., Longmire, P., Newman, B., Rogers, D., Springer, E., 1997. Performance Assessment and Composite Analysis for the Los Alamos National Laboratory Disposal Area G. Los Alamos National Laboratory document LA-UR-97-85, Report-54G-013.

Jury, W.A., Gardner, W.R., Gardner, W.H., 1991. Soil Physics. Wiley, New York.

Kersting, A.B., Effurd, D.W., Finnegan, D.L., Rokop, D.J., Smith, D.K., Thompson, J.L., 1999. Migration of plutonium in groundwater at the Nevada test site. Nature 397, 56–59.

Krier, D., Longmire, P., Gilkeson, R.H., Turin, H.J., 1997. Geologic, Geohydrologic and Geochemical Data Summary of MDA G, TA-54 Los Alamos National Laboratory. Los Alamos National Laboratory document LA-UR-95-2696.

Longmire, P., Cotter, C.R., Triay, I.R., Kitten, J.J., Hall, C., Bentley, J., Hollis, D., Adams, A.I., 1996. Batch Sorption Results for Americium, Neptunium, Plutonium, Technetium, and Uranium Transport through the Bandelier Tuff, Los Alamos, New Mexico. Los Alamos National Laboratory document LA-UR-96-4716.

Neuman, S.P., 1990. Universal scaling of hydraulic conductivities and dispersivities in geological media. Water Resour. Res. 26, 1749–1758.

Newman, B.D., 1996. Vadose Zone Water Movement at Area G, Los Alamos National Laboratory, TA-54: Interpretations Based on Chloride and Stable Isotope Profiles. Los Alamos National Laboratory document LA-UR-96-4682.

Nyhan, J.W., Drennon, B.J., Abeele, W.V., Trujillo, G., Herrera, W.J., Wheeler, M.L., Booth, J.W., Purtymun, W.D., 1984. Distribution of Radionuclides and Water in Bandelier Tuff Beneath a Former Los Alamos Liquid Waste Disposal Site after 33 Years. Los Alamos National Laboratory report LA-10159-LLWM.

Peters, R.R., Klavetter, E.A., 1988. A continuum model for water movement in an unsaturated fractured rock mass. Water Resour. Res. 24 (3), 416–430.

Purtymun, W.D., 1984. Hydrologic Characteristics of the Main Aquifer in the Los Alamos Area: Development of Groundwater Supplies. Los Alamos National Laboratory manuscript LA-9957-MS.

Purtymun, W.D., 1995. Geologic and Hydrologic Records of Observation Wells, Test Holes, Test Wells, Supply Wells, Springs, and Surface Water Stations in the Los Alamos Area. Los Alamos National Laboratory manuscript LA-12883-MS.

Rogers, M.A., 1977. History and Environmental Setting of LASL Near-Surface Land Disposal Facilities for Radioactive Wastes (Areas A, B, C, D, E, F, G, and T). Los Alamos Scientific Laboratory manuscript LA-6848-MS.

Rogers, D.B., Vold, E.L., Gallaher, B.M., 1996. Bandeher Tuff Hydraulic Characteristics from Los Alamos National Laboratory Borehole G-5 at MDA G, TA-54. New Mexico Geologic Society Guidebook, 47th Field Conference, The Jemez Mountains Region, 413–420.

Rogers, D.B., Longmire, P., Newman, B.D., Birdsell, K.H., Soll, W.E., Vold, E.L., 1997. Conceptual Model for Subsurface Transport at MDA G. Los Alamos National Laboratory report LA-UR-97-179.

Shuman, R., 1997a. Radioactive Waste Inventory for the TA-54, Area G Performance Assessment and Composite Analysis. Rogers and Associates Engineering report, RAE-9629-91B-2.

Shuman, R., 1997b. Radiological Dose Assessment for the TA-54, Area G Performance Assessment and Composite Analysis. Rogers and Associates Engineering report, RAE-9629/91B-1.

Smith, R.L., Bailey, R.A., 1966. The Bandelier Tuff: a study of ash-flow eruption cycles and zoned magma chambers. Bull. Volcanol. 29, 83–104.

Soll, W.E., Birdsell, K.H., 1998. Influence of coatings and fills on flow in fractured, unsaturated tuff porous media systems. Water Resour. Res. 34, 193–202.

Thompson, B.G.J., 1999. The role of performance assessment in the regulation of underground disposal of radioactive wastes: an international perspective. Risk Anal. 19 (5), 809–846.

Turin, H.J., 1995. Subsurface Transport Beneath MDA G: A Conceptual Model. Los Alamos National Laboratory document LA-UR-95-1663.

U.S. Department of Energy, 1998. Viability Assessment of a Repository at Yucca Mountain, Volume 3: Total System Performance Assessment. DOE report DOE/RW-0508/V3.

van Genuchten, M.T., 1980. A closed-form equation for predicting the hydraulic conductivity of unsaturated soils. Soil Sci. Soc. Am. J. 44, 892–898.

Vaniman, D., Cole, G., Gardner, J., Conaway, J., Broxton, D., Reneau, S., Rice, M., WoldeGabriel, G., Blossom, J., Goff, F., 1996. Development of a Site-Wide Geologic Model for Los Alamos National Laboratory. Los Alamos National Laboratory, LA-UR-00-2059.

Vold, E.L., Shuman, R., 1996. Phase Two of the Source Release Modeling for the Los Alamos Area G Disposal Facility Performance Assessment. Los Alamos National Laboratory report LA-UR-96-4786.

Wan, J., Wilson, J.L., 1994. Colloid transport in unsaturated porous media. Water Resour. Res. 30 (4), 857–864.

Wilson, M., Gauthier, J., Barnard, R., Barr, G., Dockery, H., Dunn, E., Eaton, R., Guerin, D., Lu, N., Martinez, M., Nilson, R., Rautman, C., Robey, T., Ross, B., Ryder, E., Schenker, A., Shannon, S., Skinner, L., Halsey, W., Gansemer, J., Lewis, L., Lamont, A., Triay, I., Meijer, A., Morris, D., 1994. Total-System Performance Assessment for Yucca Mountain — SNL Second Iteration (TSPA-1993). Sandia National Laboratory report SAND93-2675.

Zyvoloski, G.A., Robinson, B.A., Dash, Z.V., Trease, L.L., 997. Summary of the Models and Methods for the FEHM Application — A Finite Element Heat- and Mass-Transfer Code. Los Alamos National Laboratory manuscript LA-13307-MS.